Article

Electrochemical Detection of miRNA Combining T7 Exonuclease-Assisted Cascade Signal Amplification and DNA-Templated Copper Nanoparticles

Peng Miao, Tian Zhang, Jianhua Xu, and Yuguo Tang

Anal. Chem., **Just Accepted Manuscript** • DOI: 10.1021/acs.analchem.8b03425 • Publication Date (Web): 20 Aug 2018

Electrochemical Detection of miRNA Combining T7 Exonuclease-Assisted Cascade Signal Amplification and DNA-Templated Copper Nanoparticles

Peng Miao,[*,†,‡] Tian Zhang,[†,‡] Jianhua Xu,[§] and Yuguo Tang[†]

[†]Suzhou Institute of Biomedical Engineering and Technology, Chinese Academy of Sciences, Suzhou 215163, P. R. China

[‡]University of Science and Technology of China, Hefei 230026, P. R. China

[§]Department of Laboratory Science, the Second Affiliated Hospital of Guangzhou University of Chinese Medicine, Guangzhou 510120, P. R. China

* Corresponding author. Tel.: +86-512-69588279.

Email: miaopeng@sibet.ac.cn (P. M.)

ABSTRACT: miRNA has been serving as an ideal biomarker for diagnosis, prognosis and therapy of many severe diseases. In this study, we have developed an amplified electrochemical method for miRNA detection using T7 exonuclease (exo) and copper nanoparticles (CuNPs). Double-stranded DNA modified on the electrode surface are used as the template for in situ synthesis of CuNPs as excellent electrochemical signal sources. Two cycles of DNA cleavage reactions are carefully designed according to the catalytic activity of T7 exo and occur in the solution and at the electrode surface, respectively. The two cycles are integrated for cascade signal amplification. Briefly, target miRNA triggers the first cycle and its product triggers the second cycle, which destroys the template on the electrode for CuNPs synthesis. As a result, electrochemical signal is decreased and can be used to reflect the level of initial miRNA. Due to T7 exo-assisted cascade signal amplification and intense electrochemical responses from CuNPs, the biosensor is developed with excellent sensitivity. A linear range from 10^{-16} to 10^{-13} M and the limit of detection as low as 4.5×10^{-17} M are achieved. Meanwhile, it shows the capability of discriminating single base mismatch and exhibits the eligibility in the analysis of miRNA extracted from cells. Therefore, it has great potential for biomedical research and disease management.

Sensitive and selective detection of biomacromolecules has attracted tremendous interest for not only biological research but also clinical diagnosis.[1-2] To improve the analytical performances, three warrants are usually integrated including enzymes with high catalytic efficiency, ratiometric strategies based on the ratio of two independent signals, and nanomaterials with unique properties.[3-6] For example, nucleases can be used as scissors to cleave DNA at specific locus and mediate target recycling amplification;[7-8] polymerases are key components in rolling circle amplification and strand displacement amplification.[9-10] The properties of metallic nanomaterials are always not present in bulk materials or even other nanomaterials. Their excellent conductivity, high surface atom activity and quantum effects make them suitable to serve as advisable materials for analytical applications.[11-12]

miRNAs belong to non-coding endogenous RNAs which are widespread in animals, plants and microorganisms.[13-14] They participate and play a central role in gene regulation, mainly by targeting mRNAs for translational repression or cleavage.[15-16] One miRNA potentially regulates a number of genes and can significantly influence the overall regulation network.[17] Therefore, normal expression of miRNA is of great importance in various biological processes including cellular proliferation, differentiation, development and apoptosis.[18-19] miRNAs have also been implicated in various diseases,[20] including neurological, immunological and cardiovascular diseases.[21-24] Currently, many miRNAs are discussed as ideal disease biomarkers and miRNA assay is an important task not only for biomedical research, but also for early diagnosis of related diseases.[25-29]

Traditional analytical methods for the detection of miRNA include northern blotting, microarray and quantitative real-time polymerase chain reaction (qRT-PCR). However, these methods suffer certain shortcomings like high cost, tedious design, time-consuming and laborious procedure. In recent years, many other technologies have been explored for convenient miRNA assay.[30-36] For example, Fan et al. developed a versatile flow cytometric strategy for the analysis of plant miRNA combining target-templated click nucleic acid ligation and on-bead terminal DNA polymerization.[37] Miao et al. established a label-free platform for miR-155 detection based on the fluorescence quenching of gold nanoparticles (AuNPs) to silver nanoclusters (AgNCs).[38] Gu et al. utilized Au@Ag nanorods etching process for miR-141 analysis by observing surface plasmon resonance (SPR) shift.[39] Gai et al. integrated biofuel cell with a homogeneous electrochemical system to develop a self-powered miRNA biosensor.[40] Among them, electrochemical techniques are widely used in the field of bioanalysis with the advantages of high sensitivity, good selectivity, rapid response, low cost and convenient operation.[41-43]

However, there is still an increasing need for developing advanced tools for practical miRNA quantification.

In this study, we have presented a novel miRNA sensing strategy by integrating the advantages of enzyme-assisted amplification and double-stranded DNA (dsDNA)-templated copper nanoparticles (CuNPs). dsDNA is firstly immobilized on the gold electrode surface, Cu^{2+} is then adsorbed via the metal-chelating nucleobases and negatively charged phosphate backbone. Afterward, three steps are involved to form CuNPs: (1) reduction of Cu^{2+} to Cu^{+}, (2) disproportionation reaction of Cu^{+} into Cu^{2+} and Cu (0), (3) Cu (0) clustered on the dsDNA template. The application of CuNPs show several merits for electrochemical analysis.[44-45] First, DNA can be used as template for the synthesis of CuNPs with mild condition and limited duration; second, there is no strict requirements for the sequence of the dsDNA template, which facilitates different designs of biosensors; third, the in-situ preparation of CuNPs on electrode skeletons is effective, which is much superior to later immobilization process. For sensitive analysis of miRNA, T7 exonuclease (exo)-assisted cascade digestion cycles are employed. Target miRNA induces cleavage reactions, which finally destroy the DNA template for CuNPs synthesis. Potential Cu^{2+} dissolved from CuNPs could then be characterized to reveal initial miRNA level.

EXPERIMENTAL SECTION

Materials and Instruments. Potassium hexacyanoferrate (III), potassium hexacyanoferrate (II), tris(2-carboxyethyl)phosphine hydrochloride (TCEP), diethypyrocarbonate (DEPC), ethylenediaminetetraacetic acid (EDTA), mercaptohexanol (MCH), copper sulfate, 3-(N-morpholino)propane sulfonic acid (MOPS), and sodium ascorbate were obtained from Sigma-Aldrich Chemical Co. Ltd (USA). T7 exo was purchased from New England Biolabs Ltd. (Beijing, China). qRT-PCR Kit was purchased from Tiangen Biotech Co., Ltd. (Beijing, China). Other reagents were of analytical grade and used directly without further purification. DNA probes were synthesized and purified by Sangon Biotechnology Co. Ltd. (Shanghai, China). RNA probes were obtained from Takara Biotechnology Co., Ltd. (Dalian, China). The sequences were shown in Table S1. Water used in this work were prepared using a Milli Q water purification system (18 MΩ·cm resistivity) before treated with DEPC (0.1%).

Electrochemical measurements were carried out using a CHI 660D electrochemical workstation (CH Instrument, China). Transmission electron microscopic (TEM) image was taken by FEI Tecnai G20 transmission electron microscope (FEI Company, USA). Gel images were taken by a GelDoc XR+ System (Bio-Rad, USA). qRT-PCR experiments were performed on an ABI 7500 Real-Time PCR System (ABI Life Technologies, USA).

DNA Modified Gold Electrode. Before DNA modification, the substrate gold electrode was firstly treated with piranha solution (98% H_2SO_4 : 30% H_2O_2 = 3 : 1) for 5 min (*Caution: Piranha solution was highly corrosive and reacts violently with organic matter!*). Afterward, it was carefully polished to a mirror-like surface with P5000 silicon carbide paper and alumina slurries (1, 0.3, 0.05 μm), respectively. Subsequently, the electrode was cleaned by ultrasonication for 5 min in both ethanol and double-distilled water. Next, it was electrochemically cleaned with 0.5 M H_2SO_4 in order to remove any remaining materials. The electrode was dried with nitrogen and incubated with DNA probe c (0.5 μM, 10 mM Tris-HCl, 10 mM TCEP, 1 mM EDTA, 0.1 M NaCl, pH 7.4) for 8 h. After that, it was rinsed and treated with 0.1 M MCH for 0.5 h. To achieve the dsDNA probe c/d, the modified electrode was further incubated with DNA probe d (0.5 μM, 10 mM PBS, 0.2 M NaCl, pH 7.4) for 2 h.

T7 Exo-Assisted Cascade Signal Amplification. 1 μM DNA probe a and b were dissolved in 10 mM PBS (pH 7.4) containing 0.2 M NaCl, respectively. The two DNA probes were then mixed with equal volumes and heated to 95 °C for 2 min. After slowly cooled to room temperature, dsDNA probe a/b stock solution was prepared. Next, standard miRNA solutions with a series of concentrations were prepared, which were added into 10 μL of reaction solution containing 20 U T7 exo, 10 nM DNA probe a/b, 50 mM KAc, 20 mM Tris-Ac, 10 mM $Mg(Ac)_2$ and 1 mM DTT (pH 7.9). The resulted solutions were dipped on the modified electrode surface and the reactions were carried out at 37°C for 1 h.

Electrochemical Measurements. A three-electrode system was applied. A saturated calomel electrode (SCE) was used as the reference electrode, and a platinum wire was used as the counter electrode. The modified gold electrode and a glassy carbon electrode were used as working electrodes, respectively. First, cyclic voltammetry (CV) and electrochemical impedance spectroscopy (EIS) were carried out to study the electrochemical properties of DNA modified gold electrode during different steps. CV was conducted from 0.6 to -0.3 V with the scan rate of 50 mV/s. EIS was conducted upon the application of 0.192 V biasing potential and 5 mV amplitude in the frequency range of 0.1 Hz to 100 kHz. The modified gold electrode after T7 exo-catalyzed reactions was then immersed in the mixture of 200 μM Cu^{2+} and 2 mM sodium ascorbate (20 mM MOPS, 300 mM NaCl, and 2 mM $MgCl_2$) for 5 min. To measure the in-situ formed CuNPs on the gold electrode, the gold electrode was firstly dipped into 0.3 mL of HNO_3 (0.5 M) for 1 h for acid-dissolution. The solution was then added to 4.7 mL of 0.5 M HAc-NaAc buffer (pH 5.2). The blended solution was further used as the electrolyte for CV and differential pulse voltammetry (DPV) measurements. The produced Cu^{2+} was electrodeposited on the glassy carbon electrode at -1.0 V for 8 min. Then, both of CV and DPV were conducted from -0.5 to 0.2 V with the scan rate of 50 mV/s.

Cell Culture, Lysate Preparation and qRT-PCR Experiments. Human prostate cancer cells (22Rv1 and DU145), human pancreatic cancer cells (AsPc-1), human cervical cancer cells (HeLa) and human bladder cancer cells (T24) were obtained from the Institute of Biochemistry and Cell Biology, Chinese Academy of Sciences. (Shanghai, China). The five cells were cultured in RPMI 1640 medium (10% fetal bovine serum) at 37°C in a humidified 5% CO_2 incubator. After reaching a confluence of about 80%, the cells were washed, detached and collected. SingleShot™ Cell Lysis Kit was applied for the extraction according to the manufacturer's instructions. The level of target miRNA in the cell lysates were determined by the electrochemical biosensor and a commercial Quant One Step qRT-PCR Kit. Briefly, 50 μL reaction solution was prepared on ice containing 250 nM forward primer, 250 nM reverse primer, 200 nM RT primer, 200 nM TaqMan probe, 5 U of HotMaster Taq polymerase, 0.7 μL of Quant RTase, 25 μL of 2×Quant One Step Probe qRT-PCR

Master Mix and 5 μL of cell lysate. Next, it was heated to 50 °C for 30 min for reverse transcription. Afterward, the detailed PCR reaction was operated according to the manufacturer's instructions.

Scheme 1. Illustration of electrochemical biosensor for miRNA analysis based on T7 exo and DNA-templated CuNPs.

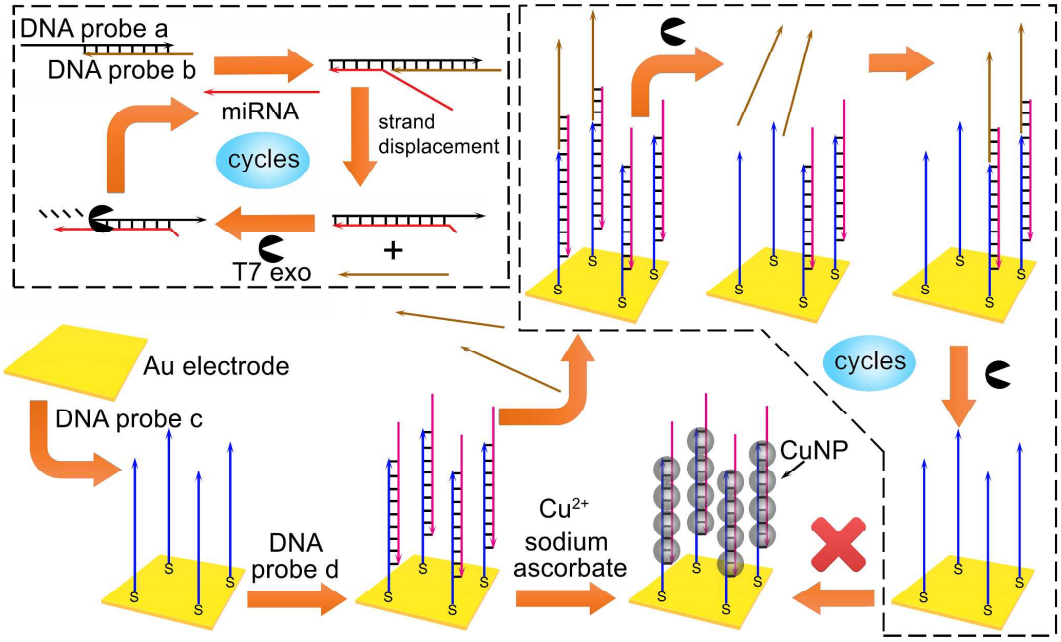

RESULTS AND DISCUSSION

Sensing Mechanism. The working principle of the proposed electrochemical biosensor for the detection of miRNA is illustrated in Scheme 1. The reaction system is consisted of target miRNA, four DNA probes and T7 exo. Hsa-miR-141 (miR-141) is chosen as a model miRNA in this work. dsDNA probe a/b is distributed in the solution while DNA probe c/d is immobilized on the surface of gold electrode due to the 5' end SH of DNA probe c. Since both of the two DNA duplexes contain 5' protruding terminuses, which are resistant to T7 exo digestion, the DNA structures are not altered. However, in the presence of target miRNA, toehold exchange-mediated strand displacement reaction occurs. The duplex of miRNA/DNA probe a forms, which contains 5' blunt terminus. Meanwhile, single-stranded DNA (ssDNA) probe b is released. Subsequently, T7 exo specifically degrades DNA probe a (5' to 3' direction) in the dupex of miRNA/DNA probe a and single-stranded miRNA is recovered. The released miRNA could trigger more cycles of strand displacement and a large number of free DNA probe b are generated. In turn, DNA probe b hybridizes with 5' end of DNA probe d in the duplex of DNA probe c/d on the electrode surface. The generated 5' recessing terminus could also be recognized by T7 exo and digestion of DNA probe d is initiated. Similarly, after complete digestion, ssDNA probe b is recovered for next cycles of hybridization and T7 exo-catalyzed cleavage of DNA probe d. Finally, a large number of dsDNA are transformed to ssDNA on the electrode. Since only dsDNA can be used as effective template for in situ synthesis of CuNPs, intense electrochemical signal variation can be obtained. An ultrasensitive biosensor for miRNA assay is thus established. Although the cascade enzymatic amplification involves two cycles of DNA cleavage reactions, a single reaction system is shared. Therefore, the amplification strategy not only has high catalytic efficiency, but also performs simply and practically. Moreover, DNA-template CuNPs exhibit facile integration with DNA-based recognition and signal amplification. The electrochemical signal sources also shows high electrochemical responses and the synthesis time can be finished within 5 min under ambient conditions. These excellent properties make CuNPs much suitable for electrochemical analysis.

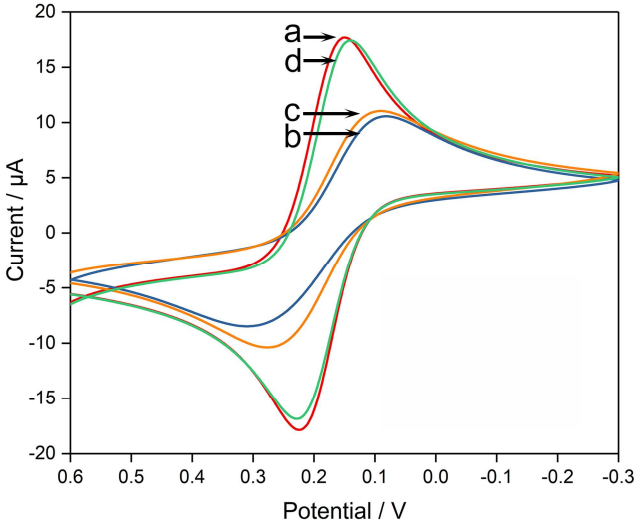

Figure 1. Cyclic voltammograms of (a) DNA probe c modified gold electrode, (b) DNA probe c/d modified gold electrode, after further treatment with T7 exo-catalyzed digestion system in the (c) absence and (d) presence of target miRNA.

Electrochemistry Behavior Characterization. Through steps of DNA immobilization and T7 exo digestion reactions, the properties of the gold electrode at different states are firstly studied by CV. As shown in Figure 1, a pair of well-defined redox peaks of $[Fe(CN)_6]^{3-/4-}$ is observed for DNA probe c modified electrode (curve a). After hybridized with DNA probe d, the electrode surface becomes more negative and repels $[Fe(CN)_6]^{3-/4-}$ more intensely, which is evidenced by the significant decrease of peak current (curve b). In the absence of miRNA, T7 exo cannot effectively degrade DNA probe d, thus the cyclic voltammogram barely changes compared with DNA probe c/d modified electrode (curve c). On the other hand, miRNA is able to trigger cascade enzymatic reactions, and a large number of DNA probe d is degraded. Therefore, the redox peak is increased with less negatively charged electrode surface, the intensity of which is on the verge of that of DNA c modified electrode (curve d).

The interfacial charge-transfer resistances during these steps are studied and compared by EIS (Figure S1). Generally, the diameter of the semicircle portion of an impedance spectrum represents the electron transfer limited process. A small semicircle is observed for DNA c modified electrode, which is increased after forming dsDNA. The diameter of the semicircle does not change significantly unless the presence of both miRNA and T7 exo. These results are consistent with those of CV.

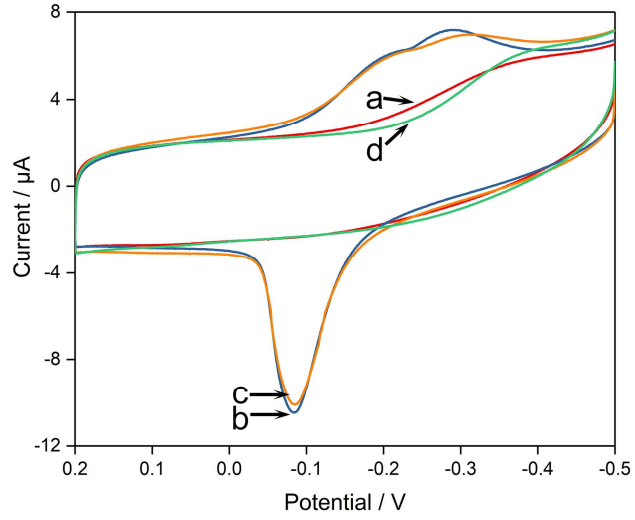

Figure 2. Cyclic voltammograms of glassy carbon electrode after electrodeposition of potential Cu^{2+} dissolved from CuNPs formed on the following DNA modified gold electrodes: (a) DNA probe c, (b) DNA probe c/d, after further treatment with T7 exo-catalyzed digestion system in the (c) absence and (d) presence of target miRNA.

Verification of the Sensing Strategy. To explore the feasibility of the proposed method, the synthesis of DNA-templated CuNPs and the T7 exo-catalyzed reactions are checked.

First, the successful synthesis of DNA-templated CuNPs can be verified by TEM. Well dispersed nanoparticles are observed with uniform size (Figure S2). The in-situ formed CuNPs on DNA probe c/d modified electrode surface can be dissolved by HNO_3 and Cu (0) is oxidized into Cu^{2+}. As shown in Figure 2 and 3, the voltammetric current peaks successfully indicate the existence or nonexistence of CuNPs, which rely on miRNA induced alterations of DNA template on the gold electrode.

Second, T7 exo-catalzyed reactions are validated by gel electrophoresis (Figure S3). The band of DNA probe a/b is not changed after T7 exo digestion in the absence of miRNA. However, after miRNA-mediated strand displacement reaction, 5' blunt terminus is generated for T7 exo digestion. A band with a smaller molecule weight appears, which is ascribed to the remained ssDNA probe b. Similarly, the band of DNA probe c/d is neither changed after T7 exo digestion in the absence of DNA probe b. Only after the hybridization with DNA probe b, 5' recessing terminus is generated for T7 exo digestion. Consequently, a smaller band of ssDNA probe c is observed.

Third, to verify the efficiency of T7 exo-assisted cascade signal amplification, we have compared the DPV peak currents of the sensing system (Figure S4). In the presence of DNA probe b directly, the peak current is much larger than using miRNA with the same concentration. The reason is as follows. miRNA triggers the first cleavage cycle and produce much more DNA probe b and the subsequent cleavage of DNA template. Less CuNPs are formed, thus the peak current intensity is much lower. The results have well demonstrated the amplification efficiency of the cascade cleavage reactions.

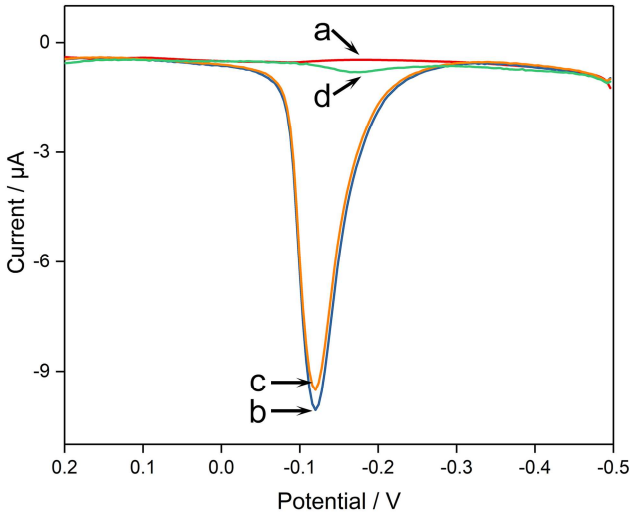

Figure 3. Differential pulse voltammograms of glassy carbon electrode after electrodeposition of potential Cu^{2+} dissolved from CuNPs formed on the following DNA modified gold electrodes: (a) DNA probe c, (b) DNA probe c/d, after further treatment with T7 exo-catalyzed digestion system in the (c) absence and (d) presence of target miRNA.

Quantitative Detection of miRNA. Before quantitative analysis of miRNA, experimental conditions are optimized by comparing the ratios of peak current or Δpeak current (Figure S5). The following parameters are chosen for the following experiments including 0.5 μM DNA probe c for gold electrode modification, -1.0 V for electrodeposition on glassy carbon electrode and 20 U T7 exo with the reaction time of 60 min for enzymatic digestion reactions. Under optimized experimental conditions, analyses are performed in triplicates for miRNA with the concentrations of 0, 10^{-16}, 2×10^{-16}, 10^{-15}, 2×10^{-15}, 10^{-14}, 10^{-13}, 10^{-12}, 10^{-11} M. The sensitivity of the method is

investigated by DPV. As explained above, the DPV peak stands for the oxidized CuNPs, which in turn reveals the miRNA level. Figure 4a depicts differential pulse voltammograms corresponding to different miRNA concentrations. As expected, larger amount of miRNA triggers more digestion of DNA template on the electrode surface, thus the peak decreases gradually. The relationship between decreased peak current and the concentration of miRNA are used for plotting calibration curves (Figure 4b). A linear relationship is established for miRNA concentration from 10^{-16} to 10^{-13} M with the equation of

$$y = -36.22 - 2.22\,x\ (n = 3,\ R^2 = 0.99)$$

in which y is the alteration of peak current and x is the logarithmic miRNA concentration. The limit of detection (LOD) is calculated to be 45 aM (signal-to-noise ratio of 3). The ultrahigh sensitivity achieved in this work is attributed not only to the T7 exo-assisted cascade signal amplification, but also to the significant electrochemical responses from DNA-templated CuNPs. The analytical performances are superior to most commercial kits and recently reported electrochemical methods (Table S2). Generally, LOD is among the lowest. The reaction time for signal amplification is relatively short. Electrochemical analysis based on DNA-templated CuNPs is also much convenient.

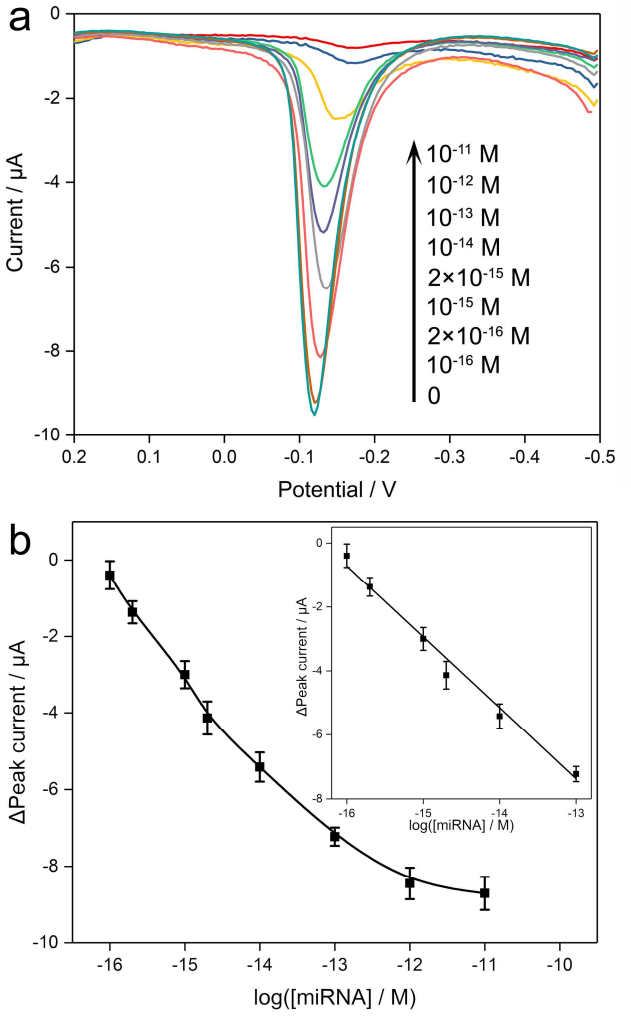

Figure 4. (a) Differential pulse voltammograms for the detection of miRNA with the concentrations of 0, 10^{-16}, 2×10^{-16}, 10^{-15}, 2×10^{-15}, 10^{-14}, 10^{-13}, 10^{-12}, 10^{-11} M (from bottom to top). (b) Calibration curve that represents the relationship between Δpeak current and logarithmic miRNA concentration. Inset shows the linear range. Error bars represent the standard deviations of three parallel tests.

Reproducibility and Selectivity Investigation. Although high sensitivity is achieved, the strategy relies on a signal turn-off mode, which may sometimes lead to false positive signals. To dissipate the suspicion, we have utilized five parallel modified gold electrodes for the detection of miRNA with the concentration of 1 fM and 0.1 pM. The relative standard deviations (RSD) are 4.52 and 2.78%, respectively, demonstrating excellent reproducibility and accuracy of this method.

Distinguishing among members from the same miRNA family is very important not only for better understanding biological mechanisms of individual miRNAs, but also for accurate disease diagnosis. We have employed five miRNAs containing single or double mismatched sites compared with target miRNA (miR-141) for comparison. As shown in Figure 5, only target miRNA can be used to trigger T7 exo-catalyzed reactions and significant electrochemical signals can be obtained. The presence of the other miRNAs only contribute to negligible signals. These results clearly demonstrate the proposed method has high sequence specificity to distinguish among miRNA family members.

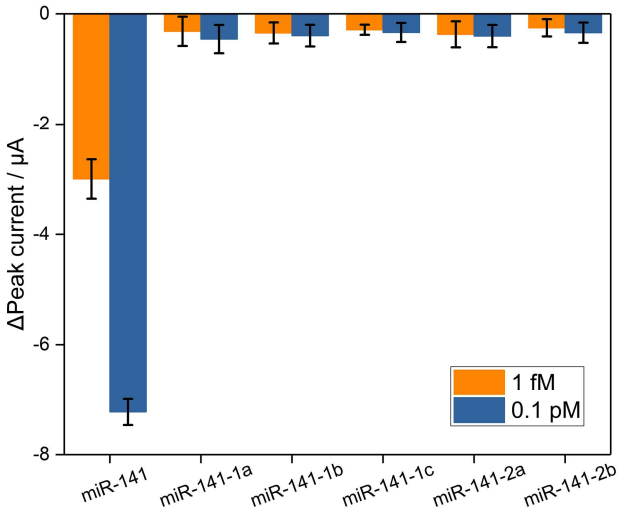

Figure 5. Specificity of the method for the detection of target miRNA. The concentrations of all miRNAs are 1 fM and 0.1 pM respectively. Error bars represent the standard deviations of three parallel tests.

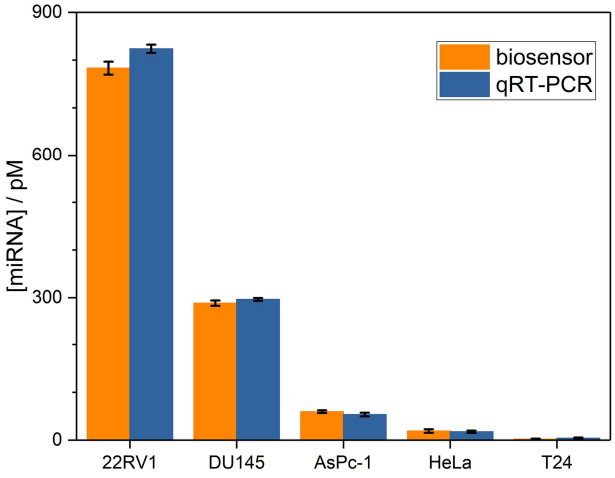

Figure 6. Practical application of miRNA detection in the lysates of different cancer cells. Error bars represent the standard deviations of three parallel tests.

Detection of miRNA in Cell Lysate. To assess the practicality of this method, five cancer cells are used as complex biological matrixes and miRNA levels in each cell lysates are determined by the proposed electrochemical biosensor and qRT-PCR method. The calculated results are shown in Figure 6. 22RV1 cells contain obvious up-regulated miR-141 level, while the concentrations in HeLa and T24 cells are relatively low. The amounts of miRNA in the five cells measured by the two methods are in good accordance with each other. The result indicates that the proposed electrochemical biosensor for miRNA analysis has great promise for practical application.

CONCLUSIONS

In summary, we have proposed a novel electrochemical sensing strategy for miRNA analysis. Taking advantages of electrochemical techniques in tracing metallic nanoparticles and T7 exo-assisted amplification, ultrasensitive detection of miRNA is achieved. Although a signal turn-off is applied, the reproducibility and accuracy are demonstrated due to the high stability of dsDNA. The proposed method can successfully discriminate target miRNA from mismatched miRNAs. It is also capable of monitoring miRNA levels in cells without sample enrichment in a highly selective manner. There results verify that this method could find potential practical applications in biomedical research and clinical diagnosis.

ASSOCIATED CONTENT

Supporting Information

The Supporting Information is available free of charge on the ACS Publications website.

EIS characterization of stepwise modification of gold electrode, TEM image of DNA-templated CuNPs, gel electrophoresis confirmation of T7 exo-catalyzed reactions, DPV confirmation of the efficiency of T7 exo-assisted amplification, optimization of experimental conditions, DNA and RNA sequences used in this study, comparison of analytical performances of recent electrochemical methods for the detection of miRNA (PDF).

AUTHOR INFORMATION

Corresponding Authors

* Email: miaopeng@sibet.ac.cn. Tel.: +86-512-69588279. (P.M.).

Author Contributions

All authors have given approval to the final version of the manuscript.

ORCID

Peng Miao: 0000-0003-3993-4778

Notes

The authors declare no competing financial interest.

ACKNOWLEDGMENT

This work is supported by the National Natural Science Foundation of China (81771929), the Science and Technology Planning Project of Guangdong Province (2014A020212274) and the Science and Technology Planning Project of Guangzhou (201510010044).

REFERENCES

(1) Mu, J.; Lin, J.; Huang, P.; Chen, X. Y., *Chem. Soc. Rev.* **2018,** *47*, 5554-5573.

(2) Yang, F.; Li, Q.; Wang, L. H.; Zhang, G. J.; Fan, C. H., *ACS Sens.* **2018,** *3*, 903-919.

(3) Miao, P.; Tang, Y. G.; Wang, B. D.; Yin, J.; Ning, L. M., *TrAC Trends Anal. Chem.* **2015,** *67*, 1-15.

(4) Yang, X.; Yang, M. X.; Pang, B.; Vara, M.; Xia, Y. N., *Chem. Rev.* **2015,** *115*, 10410-10488.

(5) Gai, P. P.; Gu, C. C.; Li, H. Y.; Sun, X. Z.; Li, F., *Anal. Chem.* **2017,** *89*, 12293-12298.

(6) Zhang, M.; Song, C. C.; Su, S.; Du, F. S.; Li, Z. C., *ACS Appl. Mater. Interfaces* **2018,** *10*, 7798-7810.

(7) Ge, L.; Wang, W. X.; Sun, X. M.; Hou, T.; Li, F., *Anal. Chem.* **2016,** *88*, 2212-2219.

(8) Miao, P.; Ning, L. M.; Li, X. X., *Anal. Chem.* **2013,** *85*, 7966-7970.

(9) Zhang, K. Y.; Lv, S. Z.; Lin, Z. Z.; Li, M. J.; Tang, D. P., *Biosens. Bioelectron.* **2018,** *101*, 159-166.

(10) Zhao, Y. X.; Chen, F.; Li, Q.; Wang, L. H.; Fan, C. H., *Chem. Rev.* **2015,** *115*, 12491-12545.

(11) Kou, B. B.; Chai, Y. Q.; Yuan, Y. L.; Yuan, R., *Anal. Chem.* **2017,** *89*, 9383-9387.

(12) Little, C. A.; Xie, R. C.; Batchelor-McAuley, C.; Kätelhön, E.; Li, X. T.; Young, N. P.; Compton, R. G., *Phys. Chem. Chem. Phys.* **2018,** *20*, 13537-13546.

(13) de Rie, D.; Abugessaisa, I.; Alam, T.; Arner, E.; Arner, P.; Ashoor, H.; Astrom, G.; Babina, M.; Bertin, N.; Burroughs, A. M.; Carlisle, A. J.; Daub, C. O.; Detmar, M.; Deviatiiarov, R.; Fort, A.; Gebhard, C.; Goldowitz, D.; Guhl, S.; Ha, T. J.; Harshbarger, J.; Hasegawa, A.; Hashimoto, K.; Herlyn, M.; Heutink, P.; Hitchens, K. J.; Hon, C. C.; Huang, E.; Ishizu, Y.; Kai, C.; Kasukawa, T.; Klinken, P.; Lassmann, T.; Lecellier, C. H.; Lee, W.; Lizio, M.; Makeev, V.; Mathelier, A.; Medvedeva, Y. A.; Mejhert, N.; Mungall, C. J.; Noma, S.; Ohshima, M.; Okada-Hatakeyama, M.; Persson, H.; Rizzu, P.; Roudnicky, F.; Saetrom, P.; Sato, H.; Severin, J.; Shin, J. W.; Swoboda, R. K.; Tarui, H.; Toyoda, H.; Vitting-Seerup, K.; Winteringham, L.; Yamaguchi, Y.; Yasuzawa, K.; Yoneda, M.; Yumoto, N.; Zabierowski, S.; Zhang, P. G.; Wells, C. A.; Summers, K. M.; Kawaji, H.; Sandelin, A.; Rehli, M.; Hayashizaki, Y.; Carninci, P.; Forrest, A. R. R.; de Hoon, M. J. L.; Consortium, F., *Nat. Biotechnol.* **2017,** *35*, 872-878.

(14) Ge, L.; Wang, W. X.; Li, F., *Anal. Chem.* **2017,** *89*, 11560-11567.

(15) Suzuki, H. I.; Young, R. A.; Sharp, P. A., *Cell* **2017,** *168*, 1000-1014.

(16) Fabian, M. R.; Sonenberg, N.; Filipowicz, W., *Ann. Rev. Biochem.* **2010,** *79*, 351-379.
(17) Carthew, R. W.; Sontheimer, E. J., *Cell* **2009,** *136*, 642-655.
(18) Aguda, B. D.; Kim, Y.; Piper-Hunter, M. G.; Friedman, A.; Marsh, C. B., *Proc. Natl. Acad. Sci. U. S. A.* **2008,** *105*, 19678-19683.
(19) Basu, P.; Kumar, G. S., *J. Photochem. Photobiol. B-Biol.* **2017,** *174*, 173-181.
(20) Keller, A.; Leidinger, P.; Bauer, A.; ElSharawy, A.; Haas, J.; Backes, C.; Wendschlag, A.; Giese, N.; Tjaden, C.; Ott, K.; Werner, J.; Hackert, T.; Ruprecht, K.; Huwer, H.; Huebers, J.; Jacobs, G.; Rosenstiel, P.; Dommisch, H.; Schaefer, A.; Muller-Quernheim, J.; Wullich, B.; Keck, B.; Graf, N.; Reichrath, J.; Vogel, B.; Nebel, A.; Jager, S. U.; Staehler, P.; Amarantos, I.; Boisguerin, V.; Staehler, C.; Beier, M.; Scheffler, M.; Buchler, M. W.; Wischhusen, J.; Haeusler, S. F. M.; Dietl, J.; Hofmann, S.; Lenhof, H. P.; Schreiber, S.; Katus, H. A.; Rottbauer, W.; Meder, B.; Hoheisel, J. D.; Franke, A.; Meese, E., *Nat. Methods* **2011,** *8*, 841-843.
(21) Victor, M. B.; Richner, M.; Olsen, H. E.; Lee, S. W.; Monteys, A. M.; Ma, C. Y.; Huh, C. J.; Zhang, B.; Davidson, B. L.; Yang, X. W.; Yoo, A. S., *Nat. Neurosci.* **2018,** *21*, 341-352.
(22) Xu, T. J.; Chu, Q.; Cui, J. X.; Zhao, X. Y., *J. Biol. Chem.* **2018,** *293*, 1386-1396.
(23) Xiao, C. C.; Rajewsky, K., *Cell* **2009,** *136*, 26-36.
(24) Xie, Z.; Wroblewska, L.; Prochazka, L.; Weiss, R.; Benenson, Y., *Science* **2011,** *333*, 1307-1311.
(25) Zhuang, J. Y.; Tang, D. P.; Lai, W. Q.; Chen, G. N.; Yang, H. H., *Anal. Chem.* **2014,** *86*, 8400-8407.
(26) Zhuang, J. Y.; Lai, W. Q.; Chen, G. N.; Tang, D. P., *Chem. Commun.* **2014,** *50*, 2935-2938.
(27) Zhang, Y.; Shuai, Z. H.; Zhou, H.; Luo, Z. M.; Liu, B.; Zhang, Y. N.; Zhang, L.; Chen, S. F.; Chao, J.; Weng, L. M.; Fan, Q. L.; Fan, C. H.; Huang, W.; Wang, L. H., *J. Am. Chem. Soc.* **2018,** *140*, 3988-3993.
(28) Hou, T.; Li, W.; Liu, X. J.; Li, F., *Anal. Chem.* **2015,** *87*, 11368-11374.
(29) Feng, C.; Mao, X. X.; Shi, H.; Bo, B.; Chen, X. X.; Chen, T. S.; Zhu, X. L.; Li, G. X., *Anal. Chem.* **2017,** *89*, 6631-6636.
(30) Miao, P.; Tang, Y. G.; Wang, B. D.; Meng, F. Y., *Anal. Chem.* **2016,** *88*, 7567-7573.
(31) Bo, B.; Zhang, T.; Jiang, Y. T.; Cui, H. Y.; Miao, P., *Anal. Chem.* **2018,** *90*, 2395-2400.
(32) Su, J.; Wang, D. F.; Norbel, L.; Shen, J. L.; Zhao, Z. H.; Dou, Y. Z.; Peng, T. H.; Shi, J. Y.; Mathur, S.; Fan, C. H.; Song, S. P., *Anal. Chem.* **2017,** *89*, 2531-2538.
(33) Zhou, Y.; Wang, H. J.; Zhang, H.; Chai, Y. Q.; Yuan, R., *Anal. Chem.* **2018,** *90*, 3543-3549.
(34) He, Y.; Yang, X.; Yuan, R.; Chai, Y. Q., *Anal. Chem.* **2017,** *89*, 8538-8544.
(35) Li, W.; Hou, T.; Wu, M.; Li, F., *Talanta* **2016,** *148*, 116-121.
(36) Miao, P.; Jiang, Y. T.; Zhang, T.; Huang, Y.; Tang, Y. G., *Chem. Commun.* **2018,** *54*, 7366-7369.
(37) Fan, W. J.; Qi, Y.; Qiu, L. Y.; He, P.; Liu, C. H.; Li, Z. P., *Anal. Chem.* **2018,** *90*, 5390-5397.
(38) Miao, X. M.; Cheng, Z. Y.; Ma, H. Y.; Li, Z. B.; Xue, N.; Wang, P., *Anal. Chem.* **2018,** *90*, 1098-1103.
(39) Gu, Y.; Song, J.; Li, M. X.; Zhang, T. T.; Zhao, W.; Xu, J. J.; Liu, M. L.; Chen, H. Y., *Anal. Chem.* **2017,** *89*, 10585-10591.
(40) Gai, P. P.; Gu, C. C.; Hou, T.; Li, F., *ACS Appl. Mater. Interfaces* **2018,** *10*, 9325-9331.
(41) Su, S.; Wu, Y.; Zhu, D.; Chao, J.; Liu, X. F.; Wan, Y.; Su, Y.; Zuo, X. L.; Fan, C. H.; Wang, L. H., *Small* **2016,** *12*, 3794-3801.
(42) Li, C.; Hu, X. L.; Lu, J. Y.; Mao, X. X.; Xiang, Y.; Shu, Y. Q.; Li, G. X., *Chem. Sci.* **2018,** *9*, 979-984.
(43) Tang, D. P.; Ren, J. J.; Lu, M. H., *Analyst* **2017,** *142*, 4794-4800.
(44) Zhao, J.; Hu, S. S.; Cao, Y.; Zhang, B.; Li, G. X., *Biosens. Bioelectron.* **2015,** *66*, 327-331.
(45) Chen, X. F.; Yang, D. W.; Tang, Y. G.; Miao, P., *Analyst* **2018,** *143*, 1685-1690.

for TOC only

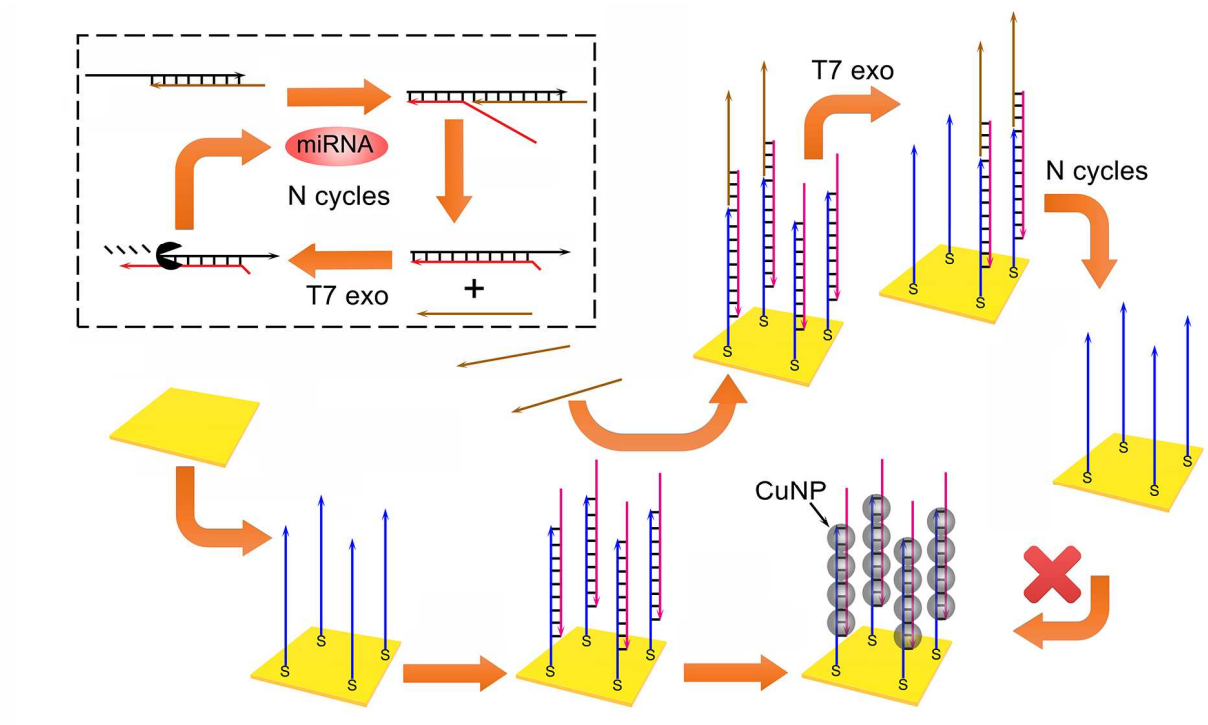

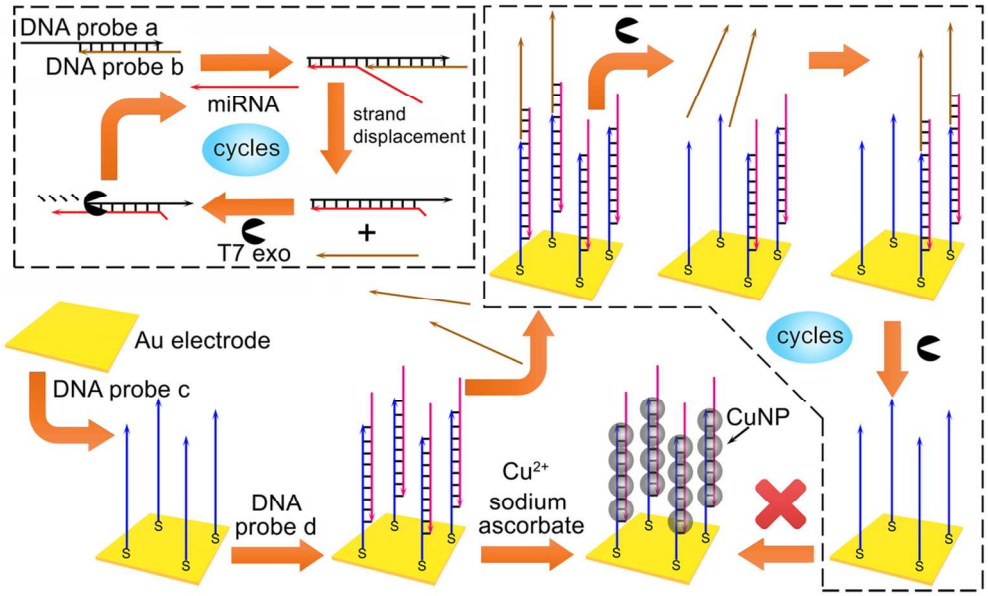

108x66mm (300 x 300 DPI)

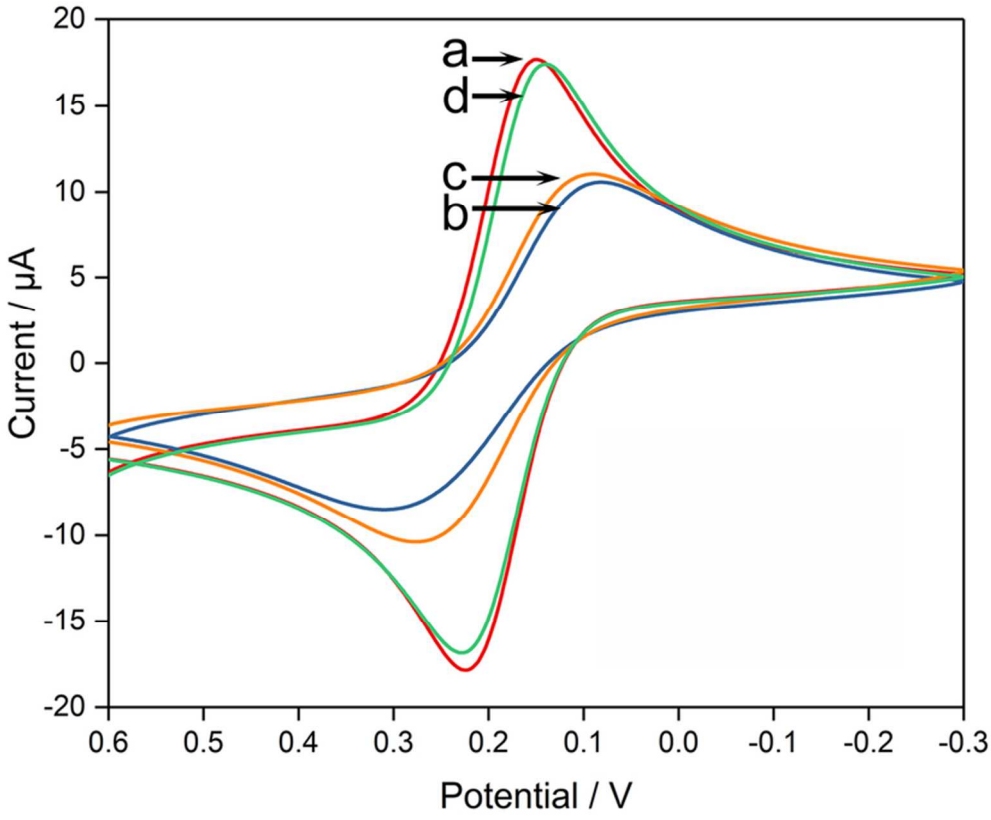

70x58mm (300 x 300 DPI)

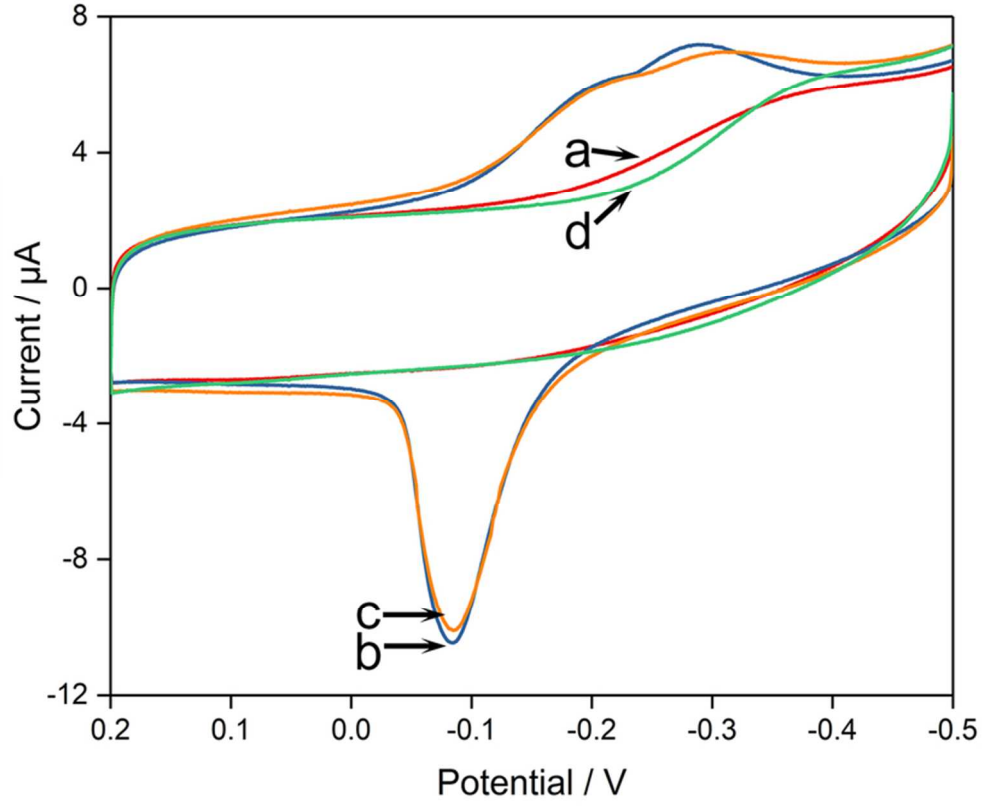

70x58mm (300 x 300 DPI)

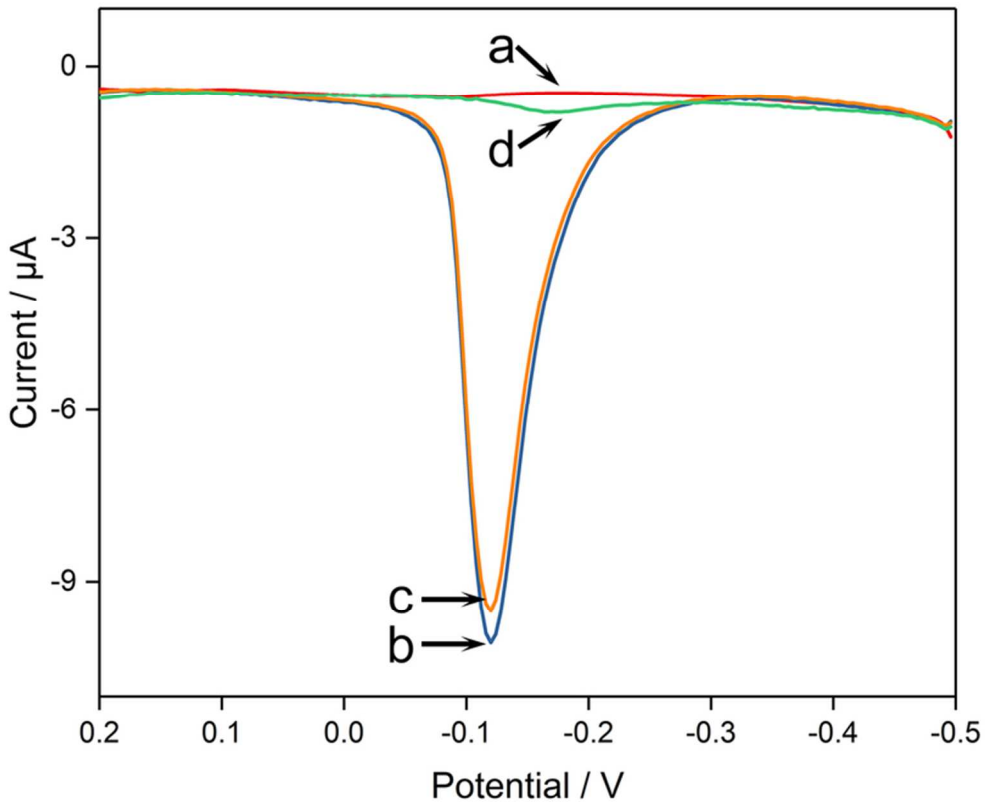

69x57mm (300 x 300 DPI)

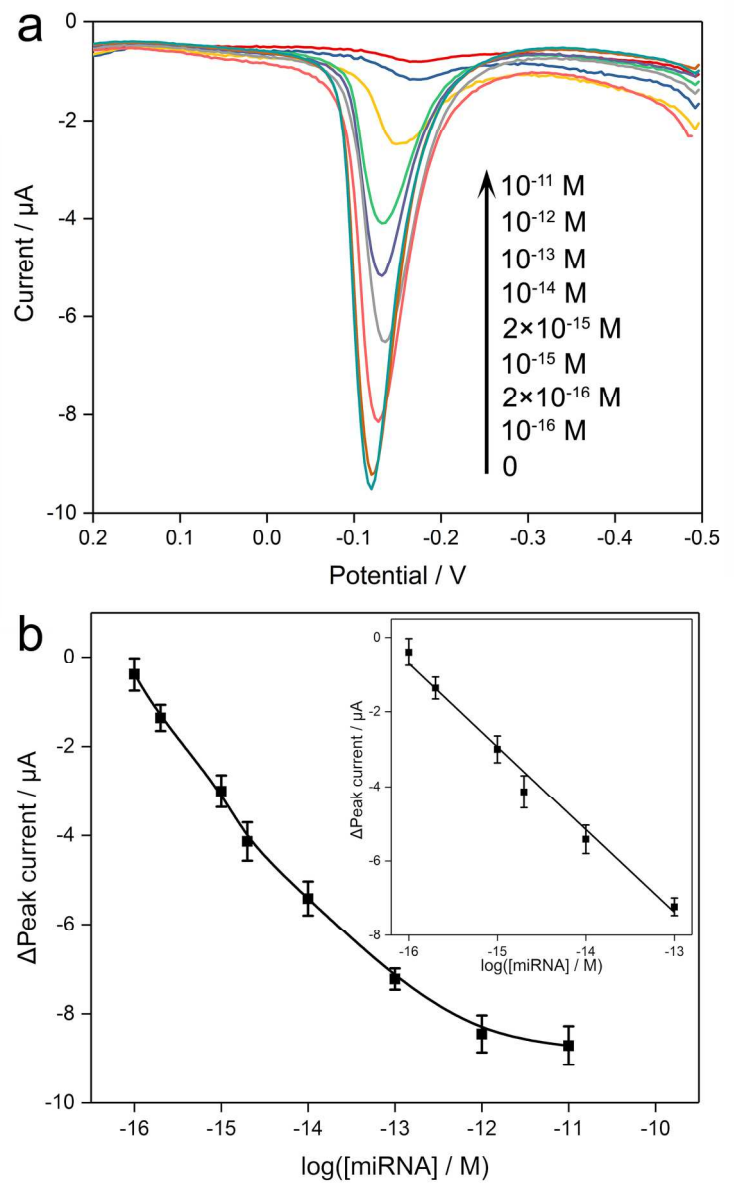

136x220mm (300 x 300 DPI)

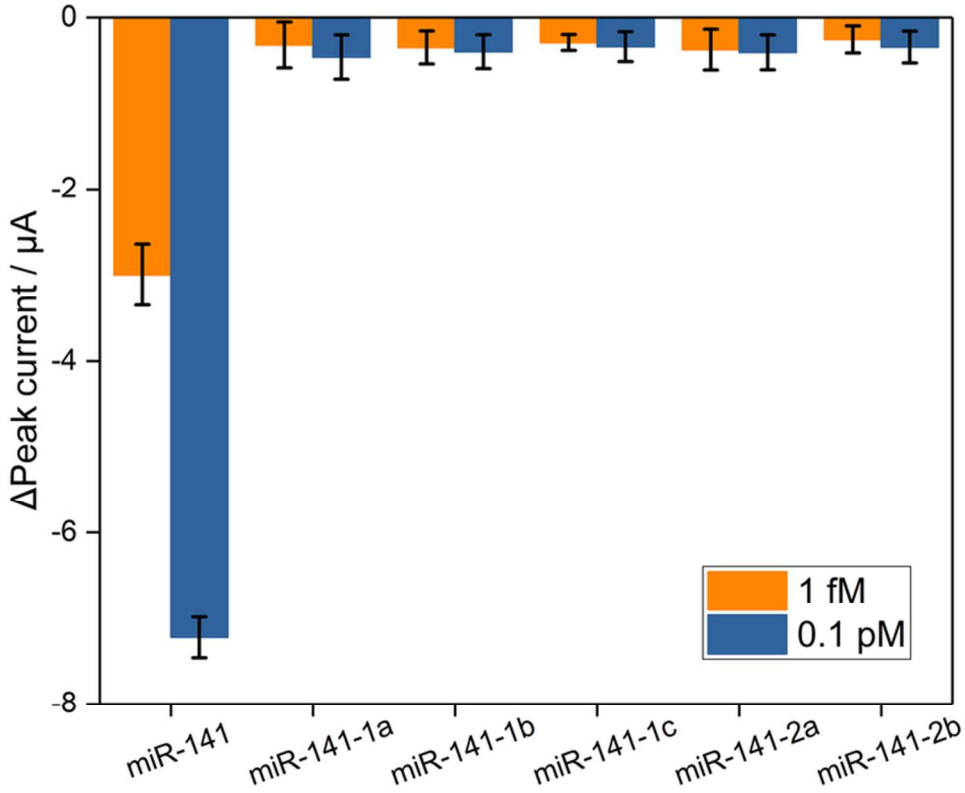

69x56mm (300 x 300 DPI)

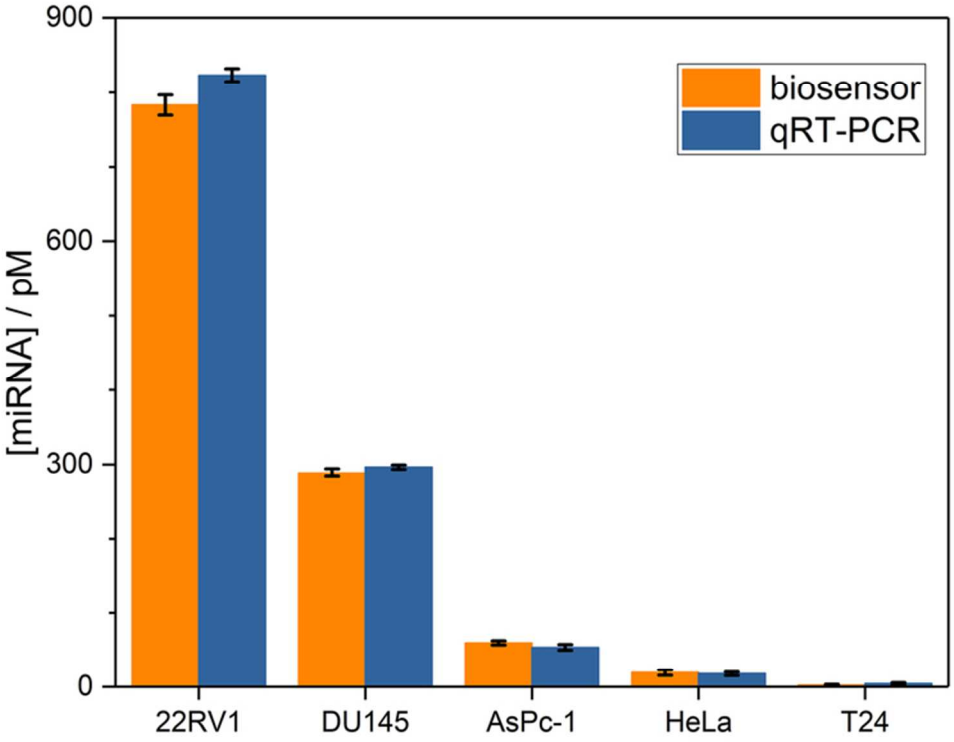

66x51mm (300 x 300 DPI)